# Hydrodynamical chemistry simulations of the Sunyaev–Zel'dovich effect and the impacts from primordial non-Gaussianities

## Francesco Pace[1]★ and Umberto Maio[2,3,4]

[1]*Institute for Cosmology and Gravitation, University of Portsmouth, Dennis Sciama Building, Portsmouth PO1 3FX, UK*

[2]*Osservatorio Astronomico di Trieste, Via G.B. Tiepolo 11, I-34143 Trieste, Italy*

[3]*Max-Planck-Institut für extraterrestrische Physik, Giessenbachstraße 1, D-85748 Garching b. München, Germany*

[4]*Leibniz-Institut für Astrophysik (AIP), An der Sternwarte 16, D-14482 Potsdam, Germany*

## ABSTRACT

The impacts of Compton scattering of hot cosmic gas with the cosmic microwave background radiation [Sunyaev–Zel'dovich (SZ) effect] are consistently quantified in Gaussian and non-Gaussian scenarios, by means of 3D numerical, *N*-body, hydrodynamic simulations, including cooling, star formation, stellar evolution and metal pollution (He, C, O, Si, Fe, S, Mg, etc.) from different stellar phases, according to proper yields for individual metal species and mass-dependent stellar lifetimes. Light cones are built through the simulation outputs and samples of 100 maps for the resulting temperature fluctuations are derived for both Gaussian and non-Gaussian primordial perturbations. From them, we estimate the possible changes due to early non-Gaussianities on SZ maps, probability distribution functions, angular power spectra and corresponding bispectra. We find that the different growth of structures in the different cases induces significant spectral distortions only in models with large non-Gaussian parameters, $f_{NL}$. In general, the overall trends are covered by the non-linear, baryonic evolution, whose feedback mechanisms tend to randomize the gas behaviour and homogenize its statistical features, quite independently from the background matter distribution. Deviations due to non-Gaussianity are almost undistinguishable for $f_{NL} \lesssim 100$, remaining always at few per cent level, within the error bars of the Gaussian scenario. Rather extreme models with $f_{NL} \sim 1000$ present more substantial deviations from the Gaussian case, overcoming baryon contaminations and showing discrepancies up to a factor of a few in the spectral properties.

**Key words:** methods: numerical – cosmology: theory – structure formation.

## 1 INTRODUCTION

In the current paradigm of cosmological structure formation, stars, galaxies and clusters of galaxies develop by gravitational collapse in an expanding space–time (e.g. Gunn & Gott 1972; Press & Schechter 1974; White & Rees 1978; Peebles 1993; Hogg 1999; Peacock 1999; Sheth & Tormen 1999; Barkana & Loeb 2001; Coles & Lucchin 2002; Peebles & Ratra 2003; Ciardi & Ferrara 2005; Bromm & Yoshida 2011), growing from primordial matter perturbations originated during the very early phases of the Universe, during the Inflation Era (Starobinsky 1980; Guth 1981; Linde 1990). Such perturbations are usually assumed to follow a Gaussian distribution (e.g. Komatsu 2010; Casaponsa et al. 2011; Curto et al. 2011; Komatsu et al. 2011; Hinshaw et al. 2013, and references therein), because of the central limit theorem. However, experimental constraints and theoretical arguments (Peebles 1983;

Desjacques & Seljak 2010; D'Amico et al. 2011; LoVerde & Smith 2011) have often questioned this assumption and supported the idea of possible deviations from pure Gaussianity. Recent analyses by the *Planck* mission (Planck Collaboration et al. 2013a,b,c) suggest small levels of non-Gaussianities, as well.

Such deviations from non-Gaussianities can be parametrized by means of a perturbative expansion of the Bardeen gauge-invariant potential (Salopek & Bond 1990; Komatsu & Spergel 2001; Desjacques & Seljak 2010; Verde 2010):

$$\Phi = \Phi_L + f_{NL} \left[ \Phi_L^2 - \left\langle \Phi_L^2 \right\rangle \right], \tag{1}$$

with $\Phi_L$ the *linear* Gaussian part, and $f_{NL}$ the dimensionless coupling constant ruling the magnitude of the deviations from Gaussianity.[1]

★ E-mail: francesco.pace@port.ac.uk

---

[1] Because $\Phi$ depends on the local value of the Gaussian field $\Phi_L$, this kind of non-Gaussianity is named local.

The effects of non-Gaussianities are expected to affect objects arisen from the evolution of high-$\sigma$ matter density fluctuations (e.g. Grinstein & Wise 1986; Koyama, Soda & Taruya 1999; Zaldarriaga 2000; Grossi et al. 2009; Wagner, Verde & Boubekeur 2010; LoVerde & Smith 2011; Pace et al. 2011; Scoccimarro et al. 2012), and, consequently, baryonic structures, primordial haloes and early protogalaxies (Maio 2011). Furthermore, non-Gaussianities can influence the cosmic star formation history (Maio & Iannuzzi 2011), the observable gamma-ray burst rate (Maio et al. 2012), metal pollution processes (Maio & Khochfar 2012) and the status of the intergalactic medium at $z \sim 3$ (Viel et al. 2009).

Since the gas can interact with the cosmic microwave background (CMB) radiation via Compton scattering between photons and free electrons (Compton 1923) during the whole cosmological evolution, the thermodynamical state of the Universe might induce imprints on the signal of time-integrated quantities, like the thermal Sunyaev–Zel'dovich (SZ) effect (Kompaneets 1956, 1957; Sunyaev & Zeldovich 1969, 1970, 1980; Birkinshaw 1999).

In fact, when integrating along the line of sight, d$l$, to estimate the CMB temperature distortions, variations in the cosmic plasma at various epochs sum up and give different contributions to the Comptonization $y$-parameter (Kompaneets 1956, 1957):

$$y = \frac{k_{\mathrm{B}}\sigma_{\mathrm{T}}}{m_{\mathrm{e}}c^2} \int n_{\mathrm{e}} T_{\mathrm{e}} \, \mathrm{d}l, \tag{2}$$

where $k_{\mathrm{B}} = 1.38 \times 10^{-16}\,\mathrm{erg\,K^{-1}}$ is the Boltzmann constant, $\sigma_{\mathrm{T}} = 6.65 \times 10^{-25}\,\mathrm{cm^2}$ is the Thomson cross-section (i.e. the low-energy limit of Compton scattering), $m_{\mathrm{e}} = 9.11 \times 10^{-28}\,\mathrm{g}$ is the electron mass, $c = 3 \times 10^{10}\,\mathrm{cm\,s^{-1}}$ is the speed of light, $n_{\mathrm{e}}$ the electron number density, $T_{\mathrm{e}}$ the corresponding temperature (much larger than the CMB temperature, $T$, in the case of interest of ionized gas) and $(n_{\mathrm{e}}\sigma_{\mathrm{T}})^{-1}$ represents the scattering mean free path. The related spectral change in the CMB temperature depends on the frequency, $\nu$ (Sunyaev & Zeldovich 1969, 1970; Birkinshaw 1999):[2]

$$\frac{\delta T}{T} = y \left[ x \coth\left(\frac{x}{2}\right) - 4 \right], \tag{3}$$

with the dimensionless parameter $x \equiv h\nu/(k_{\mathrm{B}}T)$, and $h$ Planck constant. The spectral distortion in equation (3) vanishes for $x \simeq 3.83$ (i.e. at $\nu \simeq 217\,\mathrm{GHz}$), increases for $x \gtrsim 3.83$, and decreases for $x < 3.83$. In the Rayleigh–Jeans limit at low frequencies the resulting CMB temperature variation is negative and equals

$$\frac{\delta T}{T} \sim -2y \qquad (x \ll 1). \tag{4}$$

Thus the CMB effective temperature fluctuations drops exponentially, as $\sim e^{-2y}$ (Sunyaev & Zeldovich 1970), and determines colder 'holes' in the temperature maps of microwave background radiation, associated with large structures containing hot gas (Sunyaev & Zeldovich 1972).

Quantitatively, the strength of induced CMB anisotropies will obviously depend on the amount of structures formed in the particular cosmological model considered, and will rely on the specific hydro-, chemo- and thermodynamical history expected in different models. In a large-scale cosmological context, spatially distributed

enhancements or deficits in the SZ effect could trace the underlying structure distribution. However, reliable modelling of hydro and chemical properties at different cosmic epochs is required to properly estimate thermal gas cooling and heating in different environments having different chemical compositions. Initial empirical or semi-analytical estimates of the SZ effect suggested relatively large CMB anisotropies between $\sim 10^{-3}$ (Sunyaev & Zeldovich 1980) and $\sim 10^{-5}$ (Ostriker & Vishniac 1986; Bond 1988; Cole & Kaiser 1988; Schaeffer & Silk 1988). Further, more detailed studies, relying on first numerical simulations with Gaussian initial matter perturbations ($f_{\mathrm{NL}} = 0$), gave more accurate corrections of the order of about $\sim 10^{-6}$ (Thomas & Carlberg 1989; Scaramella, Cen & Ostriker 1993; da Silva et al. 2000; Springel, White & Hernquist 2001b; Roncarelli et al. 2007; Pace et al. 2008). However, the impact of non-Gaussianities ($f_{\mathrm{NL}} \neq 0$) on the SZ effect by means of hydrodynamical, chemical simulations has not been investigated yet. The present work is, so far, the first of this type, as previous investigations have, thus, neglected effects from stellar evolution, chemical enrichment and consequent metal-dependent cooling and their interplay with the background cosmological scenario.

In the following, we will estimate the Compton $y$-parameter for models making different assumptions on the $f_{\mathrm{NL}}$ value. We will build simulated light cones (see e.g. Pace et al. 2008, and references therein) from redshift $z = 0$ to $\sim 7$ along some hundreds randomly chosen lines of sight. We will show how the SZ signal can probe the underlying matter distribution by performing a detailed analysis of the light cones obtained in different non-Gaussian, $N$-body, hydrodynamic, chemistry simulations of large-structure formation. In the simulated volumes, cooling, star formation and feedback mechanisms are addressed on the base of the local thermodynamical properties of the collapsing gas, by consistently following its density, temperature and chemical composition, and by taking into account stellar evolution for both Population III and Population II–I stars. The runs have been presented and described by Maio & Iannuzzi (2011) and we refer the interested reader to that work for further details.

A consistent inclusion of stellar evolution properties of cosmic gas (as in the simulations considered here) is extremely important when evaluating the thermal SZ effect, because the latter reflects the behaviour of gas temperatures and densities. Therefore, while dark-matter-only simulations might be ideal tools for studying clustering, mass functions (e.g. Grossi & Springel 2009; Wagner et al. 2010; Scoccimarro et al. 2012) and lensing statistics (e.g. Pace et al. 2011; Hilbert et al. 2012, and references therein), simple analytical or semi-analytical estimates derived on top of them would likely fail.

Previous studies of the effects of non-Gaussianity on SZ (see Roncarelli et al. 2010) were based exclusively on semi-analytic estimates from dark-matter-only simulations. The novelty of the present work, instead, relies on the proper accounting for hydrodynamical and chemistry evolution during structure formation, mostly concerning iron and silicon abundances, which can be significantly boosted at low $z$ by Type Ia supernova (SNIa), and carbon and oxygen species, that are expelled mainly by Type II supernova (SNII) or asymptotic giant branch (AGB) stars on short ($\sim 10^7$–$10^8\,\mathrm{yr}$) time-scales. The different delay times of these various stellar phases play a crucial role for a suitable temporal tracking of the enrichment episodes. Lack of such physical scheme would lead to severe errors in estimating the gas metal content and the consequent cooling capabilities at all epochs.

The paper is structured as follows: after presenting the simulations in Section 2, and the technique to build the light cones in

---

[2] The classical results by Sunyaev & Zeldovich (1969, 1970) are based on the non-relativistic diffusion equation by Kompaneets (1956, 1957). For a more precise approach with relativistic corrections see Fabbri (1981) and Rephaeli (1995).

**Table 1.** Initial parameters for the runs considered in this paper (from Maio & Iannuzzi 2011).

| Runs | Box side (Mpc $h^{-1}$) | Particle mass (M$_\odot$ $h^{-1}$) for gas (dark matter) | Softening (kpc $h^{-1}$) | $f_{NL}$ | Pop III IMF range (M$_\odot$) | Pop II–I IMF range (M$_\odot$) |
|------|-------------------------|----------------------------------------------------------|--------------------------|----------|-------------------------------|--------------------------------|
| Run100.0 | 100 | $3.39 \times 10^8$ ($2.20 \times 10^9$) | 7.8 | 0 | [100, 500] | [0.1, 100] |
| Run100.100 | 100 | $3.39 \times 10^8$ ($2.20 \times 10^9$) | 7.8 | 100 | [100, 500] | [0.1, 100] |
| Run100.1000 | 100 | $3.39 \times 10^8$ ($2.20 \times 10^9$) | 7.8 | 1000 | [100, 500] | [0.1, 100] |

Section 3, we will discuss the main results about SZ maps, probability distribution functions (PDFs) and power spectra in Section 4 and, finally, we will conclude in Section 5.

## 2 SIMULATIONS

We consider three simulations with different non-Gaussian parameters, described in Maio & Iannuzzi (2011), with initial conditions generated according to equation (1) with $f_{NL} = 0, 100, 1000$. Even if these non-null values of $f_{NL}$ are somewhat larger than those provided from recent measurements using the *Planck* satellite (Planck Collaboration et al. 2013c), our choice will allow us to better highlight the interplay of dark matter non-Gaussianity with gas and stellar physics. We will be able to check how relevant contaminations due to baryon evolution and feedback effects are and how much they affect the resulting SZ signal in different $f_{NL}$ models. This will give us hints about the disentanglement of possible degeneracies between the luminous and the dark sectors, as well.

The simulations were performed by using a modified version of the parallel tree/smoothed particle hydrodynamics (SPH) GADGET-3 code (Springel 2005), which included gravity and hydrodynamics, with radiative gas cooling (Sutherland & Dopita 1993; Maio et al. 2007), multiphase model for star formation (Springel & Hernquist 2003), ultraviolet (UV) background radiation (Haardt & Madau 1996), wind feedback (Aguirre et al. 2001; Springel & Hernquist 2003) and metal pollution from Population III and/or Population II–I stellar generations, all ruled by a critical metallicity threshold of $Z_{crit} = 10^{-4} Z_\odot$ (see further details in Yoshida et al. 2003; Tornatore et al. 2004, 2010; Maio et al. 2006, 2007, 2010, 2011b; Tornatore, Ferrara & Schneider 2007; Maio, Koopmans & Ciardi 2011a; Petkova & Maio 2012; Biffi & Maio 2013). We stress that in the simulations hydrodynamical quantities are self-consistently estimated by taking into account the proper yields (for He, C, O, Si, Fe, S, Mg, etc.) from stellar evolution during AGB, SNII, SNIa phases and metal-dependent (resonant and fine-structure) cooling rate for each particle and at each time-step. The initial mass function for Population II–I star formation regime is assumed to be Salpeter over the [0.1, 100] M$_\odot$ mass range, while for the Population III regime it is a power law with slope $-2.35$ over [100, 500] M$_\odot$ range.

The cosmological parameters were fixed by assuming a concordance $\Lambda$ cold dark matter ($\Lambda$CDM) model with matter-density parameter $\Omega_{m,0} = 0.3$, cosmological-density parameter $\Omega_{\Lambda,0} = 0.7$, baryon-density parameter $\Omega_{b,0} = 0.04$, expansion rate at the present epoch of $H_0 = 70 \, \text{km s}^{-1} \, \text{Mpc}^{-1}$ (i.e. normalized at $100 \, \text{km s}^{-1} \, \text{Mpc}^{-1}$, $h = 0.7$), power spectrum normalization via mass variance within 8 Mpc $h^{-1}$ radius sphere $\sigma_8 = 0.9$ and spectral index $n = 1$. The cosmological volume was sampled as a cube of 100 Mpc $h^{-1}$ side with resolution down to $\sim$kpc scales at $z \sim 0$. A schematic summary of the properties of the runs considered here is showed in Table 1. Additional details are in Maio & Iannuzzi (2011).

Gas densities and temperatures are extracted by the simulation snapshots and are projected along the line of sight to obtain three map samples for the three $f_{NL} = 0, 100, 1000$ cases, as described in the following Section 3.

## 3 LIGHT CONES THROUGH THE UNIVERSES

We build light cones by stacking the output snapshots and by following the procedure outlined in Pace et al. (2008). We make sure to cover completely the whole space from $z = 0$ to $\sim$7, and discard possibly overlapping regions from different 'adjacent' snapshots. However, a simulation is only one realization of the many possible realizations in the Universe. Thus, in order to have statistically meaningful results, it is necessary to avoid the unavoidable replication of the same structures when piling up the snapshots at different times for the same box. We reach this goal by arbitrarily reshuffling particle positions and velocities via random rotations and translations of the box axes.

As a result, for any choice of the seed of the random generator, we obtain maps showing different structure locations, but keeping, on average, the same statistical properties (Thomas & Carlberg 1989; Scaramella et al. 1993; da Silva et al. 2000; Springel, White & Hernquist 2001a; Springel et al. 2001b).

Then, at each redshift, $z$, we compute the value for $y$ in a given pixel of the map with coordinates $(i, j)$, $y^{ij}$, by discretizing equation (2) on a two-dimensional grid with (physical) cell size $L_{pix}$ (according to e.g. Thomas & Carlberg 1989; Scaramella et al. 1993; da Silva et al. 2000; Springel et al. 2001a,b; Roncarelli et al. 2007; Pace et al. 2008):

$$y^{ij} = \frac{k_B \sigma_T}{m_e c^2} \frac{V}{L_{pix}^2} \sum_k n_{e,k}^{ij} T_{e,k}^{ij} w_k^{ij}, \tag{5}$$

where $V$ is the volume discretization along the line of sight, $k$ is the summation index running over the particles in each pixel and $n_{e,k}^{ij}, T_{e,k}^{ij}, w_k^{ij}$, the corresponding electron density, temperature and projected smoothing kernel. We highlight that in the runs considered here electron fractions and temperatures are tracked on-the-fly, and can change, from particle to particle, at each time-step, according to the corresponding local metal-dependent cooling and heating rates. This is important, because in this way we get a precise estimation of $y$, taking into account the non-trivial back-reaction of star formation, feedback effects and UV background on gaseous properties.[3]

We repeat the procedure described above by choosing 100 different random lines of sight to get three map samples for each $f_{NL}$ value (and therefore we get a total of 300 maps).

We will denote these samples as: $\mathcal{S}_0$, $\mathcal{S}_{100}$ and $\mathcal{S}_{1000}$, referring to $f_{NL} = 0, 100$ and 1000, respectively.

Each map covers a field of view of $1°$.

---

[3] In this respect, post-processing estimates of dark-matter-only simulations might be misleading.
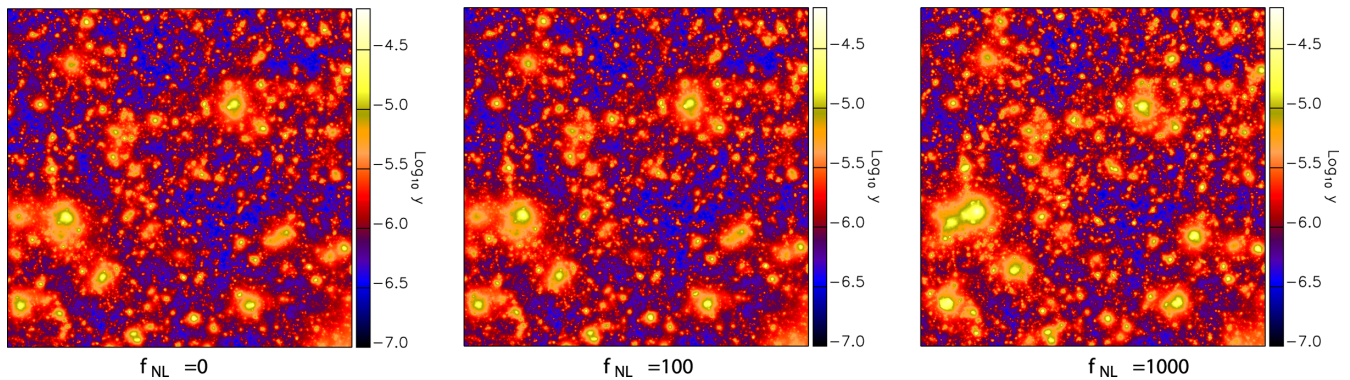
**Figure 1.** Comptonization *y*-parameter maps computed, on a grid of $1024 \times 1024$ pixels, by integrating along the same line of sight each of the three cones obtained from the models with $f_{\mathrm{NL}} = 0$ (left), $f_{\mathrm{NL}} = 100$ (centre) and $f_{\mathrm{NL}} = 1000$ (right).

In the following sections we will show the main results about the SZ effect computed for the three different $f_{\mathrm{NL}}$ models, according to the procedure just described.

## 4 RESULTS

In the following, we will first give (Section 4.1) a brief description of expected typical maps (both for the Gaussian and for the two non-Gaussian models), as obtained from the procedure outlined in Section 3, then we will consider the three full samples, each one made of 100 maps and referring to the different $f_{\mathrm{NL}}$ values considered in this work. This will allow us to analyse more carefully the statistical properties of the SZ effect and to get more solid conclusions about probability distributions (Section 4.2), power spectra (Section 4.3) and bispectra (Section 4.4).

### 4.1 Maps

In Fig. 1, we display *y*-parameter maps for the same line of sight in the three models with $f_{\mathrm{NL}} = 0$ (left), $f_{\mathrm{NL}} = 100$ (centre) and $f_{\mathrm{NL}} = 1000$ (right), as indicated by the labels. We note that the general structure and shape of the maps are quite similar, due to the fact that the same randomization process has been applied to the three cases, so the same cosmic objects broadly correspond and are easily detectable in the three panels.

While large collapsed structures are well detectable, filaments are usually not visible and covered by background signal, due to their typically lower densities and temperatures (see also discussions in e.g. da Silva et al. 2000; Springel et al. 2001a,b; White, Hernquist & Springel 2002; Zhang, Pen & Wang 2002; Roncarelli et al. 2007; Pace et al. 2008).

Because of the various non-Gaussian and Gaussian initial perturbations, the growth and evolution of different structures is slightly different. Typical values in Fig. 1 are in the range between $\sim 2 \times 10^{-7}$ and a few times $10^{-5}$, with mean values of the order of $\sim 10^{-6}$.

More specifically, the Gaussian $f_{\mathrm{NL}} = 0$ case presents a maximum *y* of $4.70 \times 10^{-5}$, while the mean is $1.67 \times 10^{-6}$. In the non-Gaussian $f_{\mathrm{NL}} = 100$ scenario, one finds a maximum of $5.13 \times 10^{-5}$, and the mean is $1.71 \times 10^{-6}$. In the non-Gaussian $f_{\mathrm{NL}} = 1000$ model, there is a maximum of $6.70 \times 10^{-5}$, and the mean is $2.05 \times 10^{-6}$. This means that, while lower values for *y* might not be significantly affected, upper values and mean values feel more the underlying distribution, from a few per cents up to tens per cent levels. The reason for that is in the fact that lower values are found in colder

environments, where the electron fraction is much smaller that unity and the effects of structure growth in boosting temperature and $n_e$ are less important.

More precisely, differences of $\sim 10$ per cent are found between $f_{\mathrm{NL}} = 1000$ and 0, with *y* values in the former case being larger because of the more advanced heating process determined by feedback effects. When considering the peak values, differences with the Gaussian model are evident in all the cases and reach about $\sim 8$ per cent for $f_{\mathrm{NL}} = 100$, and $\sim 30$ per cent for $f_{\mathrm{NL}} = 1000$. Mean values, instead, are larger than in the Gaussian case by $\sim 1.7$ per cent for $f_{\mathrm{NL}} = 100$, and by $\sim 18$ per cent for $f_{\mathrm{NL}} = 1000$.

We also mention that *y*-values do not follow a (log-)normal differential distribution, mostly because of the more extended high-$f_{\mathrm{NL}}$ tail (as previously noted by e.g. Thomas & Carlberg 1989; Scaramella et al. 1993; da Silva et al. 2000, for the Gaussian case). It is interesting that this conclusion still holds for the non-Gaussian cases (see next).

### 4.2 Probability distributions from the whole samples

In the following we will consider the whole samples of simulated maps – $\mathcal{S}_0$, $\mathcal{S}_{100}$ and $\mathcal{S}_{1000}$ – to draw more solid statistical constraints on the expected distribution of the *y*-parameter in the different scenarios.

In Fig. 2 we show our results for the differential PDF for the three models as a result of the averaging over 100 realizations. For sake of clarity, error bars, shown as a shaded region of equivalent width, are presented only for the Gaussian model (black curve) and represent $1\sigma$ deviations.

Models with $f_{\mathrm{NL}} = 100$ and 1000 are shown with red dashed and blue dotted curve, respectively. In the lower panels we show the corresponding ratio between the two non-Gaussian and the Gaussian models. The presence of primordial non-Gaussianity is mostly important for very high and unrealistic values of $f_{\mathrm{NL}}$. The non-Gaussian models present peaks in the average PDF at higher values than the Gaussian one. This is particularly evident for $f_{\mathrm{NL}} = 1000$ (blue dotted curve), while the average PDF for $f_{\mathrm{NL}} = 100$ is only slightly shifted of a few per cent. We notice that, since curves are normalized to unity, the case with $f_{\mathrm{NL}} = 1000$ shows a slightly lower peak: this is understood with the fact that this model presents higher values for the *y*-parameter – due to the predicted more massive and hotter clusters – therefore, in order to span the same area, it must have a lower peak (see Section 4.1). This result is consistent with the average values for samples. Average values are $1.34 \times 10^{-6}$ and $1.36 \times 10^{-6}$ for the $f_{\mathrm{NL}} = 0$ and 100 model, respectively, while
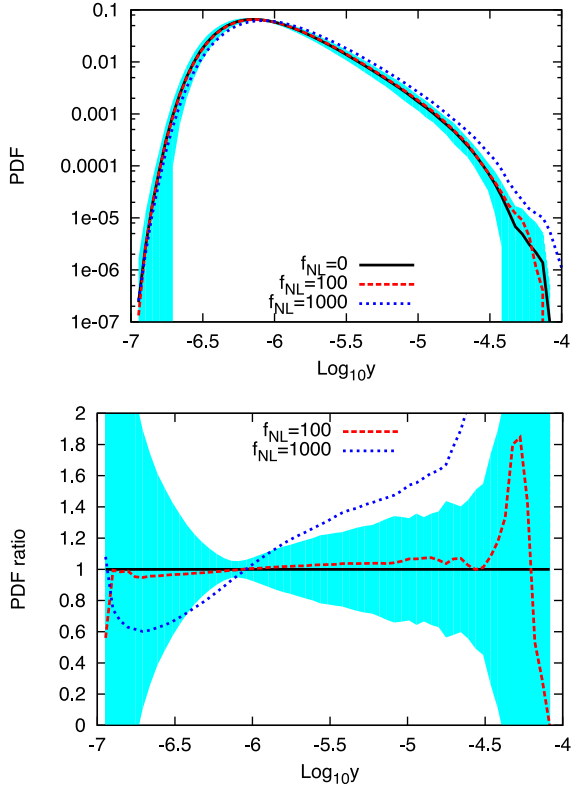
**Figure 2.** Upper panel: differential PDF for the Comptonization $y$-parameter for the three different models studied. Lower panel: ratio of the PDF between the non-Gaussian and the Gaussian model. Black line refers to the $f_{NL} = 0$ model, red dashed line to the $f_{NL} = 100$ model and the blue dotted line to the $f_{NL} = 1000$ model. The shaded region has a width equal to that of the error bars of the Gaussian model.

a higher sample average of $1.6 \times 10^{-6}$ for $f_{NL}=1000$ is reached. Thus, sample averages do not differ too much and can easily be accommodated within the error bars (see next). In addition to this, we have to take into account that measurements will suffer of uncertainties on the cosmological parameters, as well, that will be degenerate with baryon physics.

The lower panel of Fig. 2 clearly shows that, over a scale of two orders of magnitude in the Compton parameter ($-6.5 < \log_{10}(y) < -4.5$), the model with $f_{NL} = 100$ differs of at most of 5 per cent from the Gaussian one and it is well within its error bars (upper panel). This means that the two cases are basically indistinguishable. At very low and high values of the $y$-parameter, differences become substantial, but much less significant, due to poorer statistics. Larger deviations, up to a factor of a few, arise for a value of $f_{NL}$ 10 times higher, making therefore easier to distinguish this model from the reference one, in particular for high values of the Compton $y$-parameter.

We stress that gas thermal state in the different scenarios is significantly affected by the aforementioned baryonic processes that take place during cosmic structure growth (star formation, stellar evolution, metal spreading, feedback effects). These inject entropy in the surrounding medium and introduce remarkable chaotic motions in the gas, which, in turn, wash out, partly (as in the $f_{NL} = 1000$ case) or completely (as in the $f_{NL} = 100$ case), non-Gaussian signatures and are mainly responsible for a similar gas evolution within corresponding cosmic structures.

Our results are in good agreement with existing investigations of weak-lensing maps and effective-convergence studies probing

the *total* matter distribution of collapsed objects (Pace et al. 2011). Also for the effective convergence, underdense (overdense) regions show a ratio smaller (higher) than unity in non-Gaussian models with respect to the Gaussian ones, and the differences in the PDFs are comparable to the ones found here. However, due to the impacts from baryonic processes and feedback effects that tend to homogenize gas behaviour mostly for $f_{NL} \lesssim 100$, the SZ ratios in Fig. 2 (sensitive to gas) are slightly lower than effective-convergence ratios (sensitive to the total mass and thus less affected by baryons). We also note that extreme models with $f_{NL} = 1000$ present very strong deviations in both cases, as a result of a more clearly dominant contribution of the underlying dark sector over the luminous one.

In the case of the Gaussian sample, we note that our average value is slightly different than the values obtained in early works (e.g. da Silva et al. 2001; Springel et al. 2001a). This is not surprising since our simulations include much more baryonic physics than previous ones. Comparing our findings against the Gaussian model of Roncarelli et al. (2010) we note that our average values for the $y$-parameter are higher, despite the similar cosmology adopted. This is due essentially to two reasons: on the one side here we integrate our light cones up to $z \simeq 7$, while Roncarelli et al. (2010) stopped at $z \simeq 4$, on the other side differences are also partly due to the fact that here we consider several hydrodynamical processes as cooling, star formation and especially feedback (that increases temperatures quite rapidly) that in dark-matter-only simulations are not included. This highlights that high-redshift objects can still contribute to the Compton $y$-parameter when projecting along the line of sight. Therefore, our results are in better agreement with the analyses by Roncarelli et al. (2007), performed by using the hydrodynamical simulations by Borgani et al. (2004), which were integrated up to $z \approx 6$ giving $\langle y \rangle = 1.19 \times 10^{-6}$. Consequently, also the location of the PDF peak in the Gaussian scenario results in good agreement with Roncarelli et al. (2007).

Direct comparisons with other analyses of the $y$-parameter in different non-Gaussian cases are not possible as there are no related works available in literature.

### 4.3 Power spectrum from the whole samples

Given that the SZ effect contributes to the CMB power spectrum, its theoretical knowledge is of great importance. The Compton $y$-parameter power spectrum was studied in many papers (Holder & Carlstrom 1999; Komatsu & Kitayama 1999; Cooray, Hu & Tegmark 2000; Molnar & Birkinshaw 2000; Refregier et al. 2000; Seljak 2000, 2002; da Silva et al. 2001; Springel et al. 2001a; Zhang & Pen 2001; Refregier & Teyssier 2002; Zhang et al. 2002), but never with a detailed hydro, chemical treatment for gas physics and stellar evolution in non-Gaussian scenarios.

In this section we explore the effects of primordial non-Gaussianity on the expected SZ power spectrum, and we plot error bars as for the PDF case, we use a shaded region of width identical to the error bars only for the Gaussian model, since the non-Gaussian ones present error bars of comparable magnitude that will be omitted for sake of clarity. Similar to what we did for the PDF, spectra are averaged over 100 realizations and resulting standard deviations are computed. The power spectrum represents the Fourier transform of the correlation function of $y$ between $\ell_1$ and $\ell_2$ modes. It is defined as

$$\langle \hat{y}(\boldsymbol{\ell}_1)\hat{y}(\boldsymbol{\ell}_2) \rangle = (2\pi)^2 \delta_D(\boldsymbol{\ell}_1 + \boldsymbol{\ell}_2)P(\ell), \tag{6}$$

where the Dirac's delta assures that $\ell = |\boldsymbol{\ell}_1| = |\boldsymbol{\ell}_2|$.
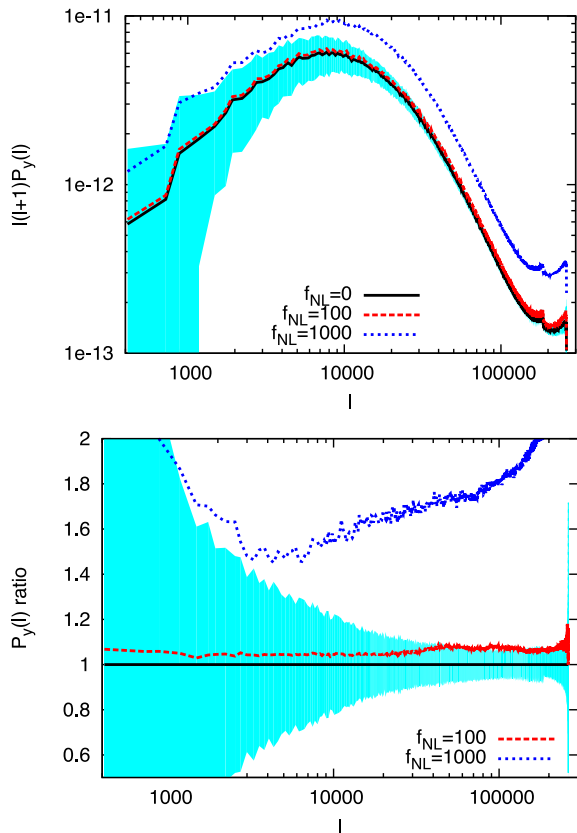
**Figure 3.** Upper panel: power spectrum for the *y*-parameter for the three different models studied. Lower panel: ratio of the power spectrum between the non-Gaussian and the Gaussian model. Black line with shaded region of width equal to the error bars refer to the $f_{NL} = 0$ model, red dashed line to the $f_{NL} = 100$ model and the blue dotted line to the $f_{NL} = 1000$ model.

The importance of the study of the SZ angular power spectrum lies in the fact that it is easier to detect than individual clusters and it is very sensitive to the underlying cosmological properties (see e.g. Komatsu & Kitayama 1999; Komatsu & Seljak 2002; Seljak 2002). Another important aspect is that it is rather insensitive to selection effects and it receives important contribution from outskirts regions of galaxy clusters, minimizing the poor knowledge of their cores.

Our results are summarized in Fig. 3, where we show average power spectra (more precisely $\ell(\ell + 1)P_y(\ell)$) for all the models (upper panel) and corresponding ratios with respect to the reference Gaussian scenario (lower panel). As expected, higher values of primordial non-Gaussianity imply stronger deviations from the power spectrum evaluated for the Gaussian model, as evident from the trends in the lower panel.

For the model with the highest amount of primordial non-Gaussianity we observe an increase of power from $\ell \approx 3000$, starting from about 50 per cent more power than the Gaussian case till a factor of 2 more power at the smallest scales ($\ell \approx 2 \times 10^5$). This is consistent with the results on the effective convergence obtained by Pace et al. (2011) in their fig. 3, as well (see discussion in the previous section). The model with $f_{NL} = 100$ differs from the Gaussian case of only 5–6 per cent at most and at every frequency available it is well within the error bars (see upper panel in Fig. 3). We stress that the error bars of Fig. 3 are bigger for lower multipoles than for higher ones, because the number of possible realizations is much smaller in the former case than in the latter one. A further comment

is necessary to discuss the shape of the ratio of the power spectra. In general, larger $f_{NL}$ values present higher power, but there are some dependencies on the particular scales considered, as rarer bigger objects are more affected by non-Gaussianities than more common smaller ones. For the simulation with $f_{NL} = 100$ the ratio with the Gaussian calculations is approximately constant, since in the $f_{NL} = 100$ and 0 scenarios statistical and physical effects are very similar and the resulting differences are not very pronounced. This is not the case for the non-Gaussian cosmology with $f_{NL} = 1000$, where we observe an evident U-shaped curve (this will happen also for the bispectrum – see Section 4.4). The increase of power at small scales (large $\ell$s) highlights the bias towards higher values of the initial perturbations in such model and the consequent higher clustering during the whole structure formation evolution. Instead the trend for multipoles of $\ell \approx$ few thousands is the result of the non-Gaussian bias. As shown in Grossi & Springel (2009), the halo bias in non-Gaussian cosmologies has a unique scale dependence: differences appear at large scales, while on smaller scales the non-Gaussian bias approaches the value of the Gaussian bias. Therefore, using gas particles to trace the underlying matter distribution, we expect to be affected by bias. This explains the declining part in the ratio between the model with $f_{NL} = 1000$ and the Gaussian case. The later increase is due to a combination of shot noise and bias due to higher clustering.

When we compare our $f_{NL} = 0$ results with the (Gaussian) power spectrum by Springel et al. (2001a) we note that the function $\ell(\ell + 1)C_\ell$ shows a peak at $\ell \approx 8000$, in agreement with what found by those authors. Our findings are instead not easily comparable with the spectrum presented in Roncarelli et al. (2010), since their highest frequency is $\ell = 10\,000$ and no peak is clearly visible in those estimates. We remind that the amplitude of the $f_{NL} = 0$ spectrum in Fig. 3 is lower than the one predicted by Springel et al. (2001a) and it is larger than the one expected by Roncarelli et al. (2010). As mentioned before, this is simply explained by taking into account the different gas physics included in our simulations with respect to the adiabatic gas of Springel et al. (2001a) and the limited redshift sample of the dark-matter-only estimates by Roncarelli et al. (2010).

Active galactic nuclei (AGN; Roychowdhury et al. 2004; Roychowdhury, Ruszkowski & Nath 2005; Scannapieco, Thacker & Couchman 2008; Battaglia et al. 2010, 2012; Prokhorov et al. 2012) might be another source of contamination when distinguishing non-Gaussian models via SZ effect since mechanical feeding from AGN can inject significant entropy into the intracluster medium (ICM). Authors found that the peak of the power spectrum is shifted towards higher (lower) $\ell$ for lower (higher) heating times and that modifications in the power spectrum are small for $\ell \lesssim 2000$, while they increase for higher multipoles, where a substantial reduction of the power at small angular scales was noticed. Moreover, the high-multipole range is very sensitive to the particular feedback recipe used. Whatever the particular prescription (e.g. Scannapieco et al. 2008; Battaglia et al. 2010, 2012; Prokhorov et al. 2012) adopted in the runs, this will be the same gas-heating phenomenon acting in all the various cosmological models, independently from $f_{NL}$. Hence, the consequent boost of the chaotic state of the IGM will increase the level of degeneracy among possible $f_{NL}$ values and further erase gaseous signatures of primordial non-Gaussianities – as any other feedback effect would do (Maio 2011; Maio & Iannuzzi 2011; Maio & Khochfar 2012). The resulting *y* distributions and spectra could suffer of systematic shifts, however, their ratio is expected to converge to the Gaussian behaviour more rapidly. Effects of non-Gaussianity on the power spectrum were analysed by Hill &

Pajer (2013). In this work the authors used the halo model approach to evaluate the thermal SZ power spectrum signal and estimated the influence of non-Gaussianity with modifications of the mass function and of the halo bias. Hill & Pajer (2013) found that the effect of non-Gaussianity is approximately constant and of the order of $\sim 10$ per cent, in agreement with our findings, confirming that the major contribution is coming from the different cosmological evolution of structures and that it is not feasible to constrain $f_{NL}$ using thermal SZ measurements at the present time.

It is worth saying that our conclusions on the ratio of the power spectra might be affected by errors on the precise cosmological parameters due to the scaling of the Compton parameter and of the power spectrum with $\Omega_m$ and $\sigma_8$, according to (Komatsu & Seljak 2002; Diego & Majumdar 2004; Roncarelli et al. 2010) $y \propto \Omega_m \sigma_8^{3.5}$ and $C_\ell \propto \Omega_m^2 \sigma_8^7$. This means that small uncertainties in the cosmological parameters might strongly impact the expected results and get degenerated with realistic values of primordial non-Gaussianity.

## 4.4 Bispectrum from the whole samples

While Gaussian fields are entirely described by the PDF and the power spectrum (higher order moments are null), this is not true anymore for non-Gaussian models, that, to be entirely characterized, would require the knowledge of all higher moments, corresponding to the so-called polyspectra in the Fourier space.

In the following we will focus on the bispectrum, because it is related to the first non-null moment and possibly carries most of the physical information of non-Gaussian scenarios. Furthermore, it is a very useful quantity to constrain cosmological parameters, especially in combination with the power spectrum, and can help disentangle the effects of gravity from the effects of biasing (see e.g. Verde et al. 1998; Verde, Heavens & Matarrese 2000; Takada & Jain 2004; Sefusatti et al. 2006; Sefusatti, Crocce & Desjacques 2010; Pace et al. 2011).

Compared to the power spectrum, the bispectrum depends on three frequencies such that in the Fourier space they form a triangular configuration. The evaluation of the bispectrum for each single configuration is computationally expensive, therefore, we limit ourselves to the study of the equilateral configuration in which all the three frequencies are assumed to be the same.

The bispectrum of the Compton parameter $y$ is defined as

$$\langle \hat{y}(\boldsymbol{\ell}_1)\hat{y}(\boldsymbol{\ell}_2)\hat{y}(\boldsymbol{\ell}_3) \rangle = (2\pi)^2 \delta_D(\boldsymbol{\ell}_{123})B(\ell_1, \ell_2, \theta_{12}). \tag{7}$$

To form a triangle in the Fourier space, we require that $\boldsymbol{\ell}_1 + \boldsymbol{\ell}_2 + \boldsymbol{\ell}_3 = \mathbf{0}$. In the previous equation, $\theta_{12}$ represents the angle between $\boldsymbol{\ell}_1$ and $\boldsymbol{\ell}_2$, which, together with the triangle condition, fixes $\boldsymbol{\ell}_3$.

We show our results in Fig. 4. In the upper panel we present the comparison of the bispectra for the three different models studied, while in the lower panel we show the ratio between the bispectrum of the non-Gaussian models and that of the Gaussian model.

The trends are similar to what found for the power spectrum, with relative differences increasing with the primordial non-Gaussianity parameter. Ratios between non-Gaussian and Gaussian bispectra are higher than the ones relative to the power spectrum since higher order spectra are more sensitive to deviations from Gaussianity than the power spectrum. For the most extreme $f_{NL} = 1000$ case the ratios at various scales range within a factor of 1.7–4, instead for the model with $f_{NL} = 100$ there is a roughly constant enhancement of $\approx 10$–12 per cent, that, nevertheless, is still within the error bars of the Gaussian $f_{NL} = 0$ case.
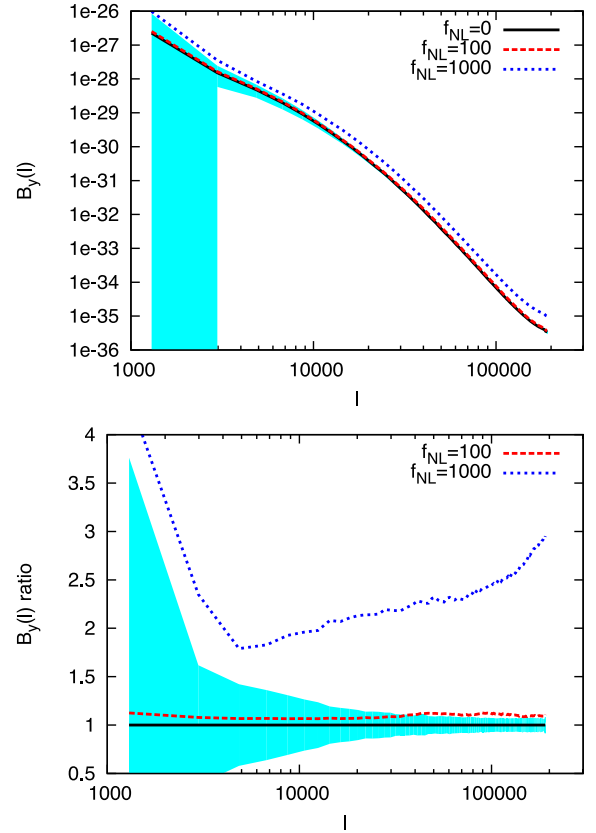


**Figure 4.** Upper panel: bispectrum (BS) with an equilateral configuration for the $y$-parameter for the three different models studied. Lower panel: ratio of the BS between the non-Gaussian and the Gaussian model. Black line with shaded region of width equal to the error bars refers to the $f_{NL} = 0$ model, red dashed line to the $f_{NL} = 100$ model and the blue dotted line to the $f_{NL} = 1000$ model.

While for the case of the power spectrum even the model with the highest amount of non-Gaussianity considered was not so different from the Gaussian reference, for the bispectrum this is not the case anymore. In fact, we see that (upper panel of Fig. 4) the bispectrum for the $f_{NL} = 1000$ initial conditions is clearly off the error bars at all the scales probed in our simulations. This because the bispectrum is very sensitive to non-linearities and to clustering properties, which are enhanced in the $f_{NL} = 1000$ model. Moreover, physically, the bispectrum is expected to scale as the square of the power spectrum and this explains values and shapes of the lower panel in Fig. 4, compared to Fig. 3 (see also discussion in Section 4.3).

Theoretical derivation of the bispectrum for the thermal SZ (tSZ) effect has been recently carried out by Bhattacharya et al. (2012). The authors use the halo model approach, as done by Komatsu & Seljak (2002) for the SZ power spectrum. According to their derivation, the bispectrum is extremely sensitive to the matter power spectrum normalization ($B_{tSZ} \propto \sigma_8^{11-12}$) and to the baryon density ($B_{tSZ} \propto \Omega_b^4$). This has positive and negative aspects. The positive aspect is that a combined use of the tSZ spectra (power spectrum and bispectrum) will help to reduce the uncertainties on cosmological parameters. On the other side, such a steep dependence on the normalization is such that a small error on $\sigma_8$ will have catastrophic consequences on the bispectrum normalization. In other words, as shown also in Pace et al. (2011), the uncertainty on the cosmological parameters has by far bigger effects than primordial non-Gaussianity, usually overcoming it.

Now suppose instead that all the cosmological parameters are perfectly known. The major uncertainty comes from gas physics and in particular from AGN feedback. Bhattacharya et al. (2012) estimated a ∼33 per cent uncertainty on the overall amplitude of the tSZ bispectrum, see their fig. 5. As it looks clear from the lower panel in our Fig. 4, errors of the order of ∼33 per cent in the amplitude will generically be within the error bars inferred from the different realizations up to $\ell \simeq 10^4$ and will become progressively more important with the increase of the multipole. We also notice that therefore the uncertainty due the gas physics will be more important than the effect of primordial non-Gaussianity, at least for $f_{NL}$ = 100. This shows clearly how important is the correct inclusion of gas physics. Recent theoretical studies Hill & Sherwin (2013) also evaluated the importance of the real-space statistics of the thermal SZ effect, in evaluating in particular the variance and the skewness, showing that a particular combination of the two ($|\langle T^3 \rangle / \langle T^2 \rangle^{1.4}|$) can remove much of the dependence on cosmology (in particular $\sigma_8$).

To date, the only known, at least to us, observational results on the tSZ bispectrum come from the *Planck* analysis (Planck Collaboration et al. 2013d) and the SPT collaboration (Crawford et al. 2013), while the ACT collaboration measured the skewness (the real-space analogue of the bispectrum; Wilson et al. 2012). In fig. 11 of Planck Collaboration et al. (2013d), the authors show the bispectrum for $100 \lesssim \ell \lesssim 700$ for four different configurations, equilateral, orthogonal and flat isosceles and squeezed. A direct comparison is impossible due to the different multipoles probed here, as our bispectrum is evaluated for $\ell > 1000$. Nevertheless, despite this and the very large uncertainties, we can estimate that the amplitude of the bispectrum is comparable for both curves, making therefore our results stronger. Also we cannot directly compare our results for the bispectrum with the ones by Wilson et al. (2012), due to the different matter power spectrum normalizations.

# 5 DISCUSSION AND CONCLUSIONS

In this work we have addressed the SZ effect and the possible implications from primordial non-Gaussianities, by using suited *N*-body, hydrodynamical, chemistry simulations (Maio & Iannuzzi 2011). The runs include dark matter dynamics and gas hydrodynamics, metallicity-dependent resonant and fine-structure cooling, star formation, feedback, stellar evolution and metal spreading according to the proper stellar yields and lifetimes. As primordial non-Gaussianities are likely to impact the formation and evolution of dark matter high-$\sigma$ objects and, hence, the whole baryonic star formation process of high-$z$ gas, induced deviations in temperatures and densities would add up when integrating along the line of sight and possibly show up in the behaviour of the SZ signal at $z \sim 0$.

To check these issues, we build up different samples of 100 simulated light cones, extracted from runs of structure formation and evolution in Gaussian $f_{NL}$ = 0 initial conditions and non-Gaussian, $f_{NL}$ = 100 and 1000 initial conditions. We obtain $y$-parameter maps and study PDFs, power spectra and bispectra in the different cosmological scenarios.

In general, for mild variations from Gaussianities – i.e. $f_{NL} \lesssim 100$ – the SZ signal varies by few per cent, while for larger variations – $f_{NL} \sim 1000$ – resulting discrepancies are much more visible and can reach a factor of a few.

Minimum $y$ values are found to be not significantly affected by primordial non-Gaussianities, while mean and upper values retain some influence by the underlying matter distribution (see discussion in Sections 4.1 and 4.2).

These results are validated by a more general investigation of the PDF functions of the Compton parameter, $y$ (Fig. 2). The $y$ distribution for the case of $f_{NL}$ = 100 is within the error bars of the Gaussian model, instead for larger values of $f_{NL} \sim 1000$ differences are more substantial.

We also stressed that the contribution of sources at $z > 4$ is important to correctly estimate the SZ signal (see discussion in Section 4.2).

The SZ power spectrum (Fig. 3) in a model with $f_{NL}$ = 100 differs only of few per cent from a Gaussian scenario and differences are within 1$\sigma$ error bars, making the two models not easily distinguishable. Similar conclusions apply, in general, to cases with $0 < f_{NL} < 100$. In a model with 10 times more primordial non-Gaussianity the underlying matter distribution and growth have a more significant impact on the SZ signal at all scales probed, achieving ∼50 per cent or more enhancement with respect to the model with $f_{NL}$ = 0. Because of the detailed gas and chemical treatments, we find that, although the peak in the $f_{NL}$ = 0 angular power spectrum is consistent with early analyses (e.g. Springel et al. 2001a), the amplitude is lower, but in agreement with more recent estimates in Gaussian scenarios (e.g. Roncarelli et al. 2007).

The bispectrum shows a stronger signal with deviations with respect to the reference Gaussian case reaching ∼10–12 per cent for $f_{NL}$ = 100 and even a factor of a few for the $f_{NL}$ = 1000 case (Fig. 4). At the same time, also error bars are bigger, and models with low $f_{NL}$ values remain compatible with the $f_{NL}$ = 0 case. These results are roughly consistent with the behaviour of the effective-convergence power spectra and bispectra in non-Gaussian models, as well (see Pace et al. 2011, for a deeper discussion), although weak-lensing statistics is quite insensitive to baryon physics and show more distinct behaviours for the different $f_{NL}$ scenarios. As shown by Bhattacharya et al. (2012), the tSZ bispectrum is very sensitive to the matter power spectrum and its amplitude is greatly affected by the AGN feedback. This means that effects of primordial non-Gaussianity will be overcome by the uncertainties in the knowledge of the cosmological parameter and in the gas physics, making therefore impossible to infer something for low values of primordial non-Gaussianity. Thanks to the ACT (Wilson et al. 2012) and the SPT (Crawford et al. 2013) collaborations and the *Planck* satellite (Planck Collaboration et al. 2013d) it is now possible to evaluate observationally the SZ bispectrum, but due to the small size of our simulated box and the different power spectrum normalization we cannot make a direct comparison since the multipoles probed in our work do not cover the observed ones. Despite this we notice that amplitudes of the bispectra around $\ell \simeq 1000$ are very similar.

An aspect to be taken into account is the degeneracy with cosmological parameters. Indeed, the SZ power spectrum depends both on the matter density, $\Omega_m$, and, much more strongly, on the matter power spectrum normalization, $\sigma_8$, according to $C_\ell \propto \Omega_m^2 \sigma_8^7$ (e.g. Komatsu & Seljak 2002; Diego & Majumdar 2004). Thus, small uncertainties on $\sigma_8$ will affect the determination of $P(y)$ and error estimation of cosmological parameters could dominate the effects of intrinsic non-Gaussianity (Pace et al. 2011). In this respect, also baryonic physics might be a severe source of contaminations, as e.g. primordial streaming motions could delay early star formation events and consequently alter the whole thermodynamic of collapsed objects at early times, introducing more degeneracies with $f_{NL}$ (Maio 2011). Furthermore, stellar evolution and the final fates of stars are responsible for injecting huge amounts of entropy in the gas over cosmological times, directly impacting the resulting SZ signal. As a consequence, our lack of knowledge about detailed

stellar parameters yields initial mass function for different populations, feedback effects from different kind of stars, etc. might have some effects. However, given the randomizing role of all these mechanisms, their influence should go in the direction outlined in this work, mostly for $f_{NL} \lesssim 100$ models.

In conclusion, what emerges clearly from our analyses is that implications from primordial non-Gaussianities on the SZ effect are strongly dependent on $f_{NL}$ with larger impacts for larger $f_{NL}$ values. Scenarios in which $f_{NL} \lesssim 100$ are almost undistinguishable from the Gaussian counterpart. Indeed, in these cases, the trends for the $y$ parameter PDFs, spectra and bispectra lie within the error bars of the Gaussian case and the discrepancies are only at a few per cent level. More extreme models with larger $f_{NL}$ values ($\sim 1000$) present more substantial deviations from the Gaussian case with discrepancies up to a factor of a few.

## ACKNOWLEDGEMENTS

## REFERENCES

Aguirre A., Hernquist L., Schaye J., Katz N., Weinberg D. H., Gardner J., 2001, ApJ, 561, 521
Barkana R., Loeb A., 2001, Phys. Rep., 349, 125
Battaglia N., Bond J. R., Pfrommer C., Sievers J. L., Sijacki D., 2010, ApJ, 725, 91
Battaglia N., Bond J. R., Pfrommer C., Sievers J. L., 2012, ApJ, 758, 75
Bhattacharya S., Nagai D., Shaw L., Crawford T., Holder G. P., 2012, ApJ, 760, 5
Biffi V., Maio U., 2013, MNRAS, preprint (arXiv:1309.2283)
Birkinshaw M., 1999, Phys. Rep., 310, 97
Bond J. R., 1988, in Unruh W. G., Semenoff G. W., eds, NATO ASIC Proc. 219, The Early Universe. Reidel, Dordrecht, p. 283
Borgani S. et al., 2004, MNRAS, 348, 1078
Bromm V., Yoshida N., 2011, ARA&A, 49, 373
Casaponsa B., Bridges M., Curto A., Barreiro R. B., Hobson M. P., Martínez-González E., 2011, MNRAS, 416, 457
Ciardi B., Ferrara A., 2005, Space Sci. Rev., 116, 625
Cole S., Kaiser N., 1988, MNRAS, 233, 637
Coles P., Lucchin F., 2002, Cosmology: The Origin and Evolution of Cosmic Structure, 2nd edn. Wiley, New York
Compton A. H., 1923, Phys. Rev., 21, 483
Cooray A., Hu W., Tegmark M., 2000, ApJ, 540, 1
Crawford T. M. et al., 2013, preprint (arXiv:1303.3535)
Curto A., Martínez-González E., Barreiro R. B., Hobson M. P., 2011, MNRAS, 417, 488
D'Amico G., Musso M., Noreña J., Paranjape A., 2011, Phys. Rev. D, 83, 023521
da Silva A. C., Barbosa D., Liddle A. R., Thomas P. A., 2000, MNRAS, 317, 37
da Silva A. C., Kay S. T., Liddle A. R., Thomas P. A., Pearce F. R., Barbosa D., 2001, ApJ, 561, L15

Desjacques V., Seljak U., 2010, Classical Quantum Gravity, 27, 124011
Diego J. M., Majumdar S., 2004, MNRAS, 352, 993
Fabbri R., 1981, Ap&SS, 77, 529
Grinstein B., Wise M. B., 1986, ApJ, 310, 19
Grossi M., Springel V., 2009, MNRAS, 394, 1559
Grossi M., Verde L., Carbone C., Dolag K., Branchini E., Iannuzzi F., Matarrese S., Moscardini L., 2009, MNRAS, 398, 321
Gunn J. E., Gott J. R., III, 1972, ApJ, 176, 1
Guth A. H., 1981, Phys. Rev. D, 23, 347
Haardt F., Madau P., 1996, ApJ, 461, 20
Hilbert S., Marian L., Smith R. E., Desjacques V., 2012, MNRAS, 426, 2870
Hill J. C., Pajer E., 2013, Phys. Rev. D, 88, 063526
Hill J. C., Sherwin B. D., 2013, Phys. Rev. D, 87, 023527
Hinshaw G. et al., 2013, ApJS, 208, 19
Hogg D. W., 1999, preprint (astro-ph/9905116)
Holder G. P., Carlstrom J. E., 1999, in de Oliveira-Costa A., Tegmark M., eds, ASP Conf. Ser. Vol. 181, Microwave Foregrounds. Astron. Soc. Pac., San Francisco, p. 199
Komatsu E., 2010, Classical Quantum Gravity, 27, 124010
Komatsu E., Kitayama T., 1999, ApJ, 526, L1
Komatsu E., Seljak U., 2002, MNRAS, 336, 1256
Komatsu E., Spergel D. N., 2001, Phys. Rev. D, 63, 063002
Komatsu E. et al., 2011, ApJS, 192, 18
Kompaneets A. S., 1956, Zh. Eksp. Teor. Fiz., 31, 876
Kompaneets A. S., 1957, Sov. Phys. JETP, 4, 730
Koyama K., Soda J., Taruya A., 1999, MNRAS, 310, 1111
Linde A., 1990, Phys. Lett. B, 238, 160
LoVerde M., Smith K. M., 2011, J. Cosmol. Astropart. Phys., 8, 3
Maio U., 2011, Classical Quantum Gravity, 28, 225015
Maio U., Iannuzzi F., 2011, MNRAS, 415, 3021
Maio U., Khochfar S., 2012, MNRAS, 421, 1113
Maio U., Dolag K., Meneghetti M., Moscardini L., Yoshida N., Baccigalupi C., Bartelmann M., Perrotta F., 2006, MNRAS, 373, 869
Maio U., Dolag K., Ciardi B., Tornatore L., 2007, MNRAS, 379, 963
Maio U., Ciardi B., Dolag K., Tornatore L., Khochfar S., 2010, MNRAS, 407, 1003
Maio U., Koopmans L. V. E., Ciardi B., 2011a, MNRAS, 412, L40
Maio U., Khochfar S., Johnson J. L., Ciardi B., 2011b, MNRAS, 414, 1145
Maio U., Salvaterra R., Moscardini L., Ciardi B., 2012, MNRAS, 426, 2078
Molnar S. M., Birkinshaw M., 2000, ApJ, 537, 542
Ostriker J. P., Vishniac E. T., 1986, ApJ, 306, L51
Pace F., Maturi M., Bartelmann M., Cappelluti N., Dolag K., Meneghetti M., Moscardini L., 2008, A&A, 483, 389
Pace F., Moscardini L., Bartelmann M., Branchini E., Dolag K., Grossi M., Matarrese S., 2011, MNRAS, 411, 595
Peacock J. A., 1999, Cosmological Physics. Cambridge Univ. Press, Cambridge
Peebles P. J. E., 1983, ApJ, 274, 1
Peebles P. J. E., 1993, Principles of Physical Cosmology. Princeton Univ. Press, Princeton, NJ
Peebles P. J., Ratra B., 2003, Rev. Modern Phys., 75, 559
Petkova M., Maio U., 2012, MNRAS, 422, 3067
Planck Collaboration et al., 2013a, preprint (arXiv:1303.5075)
Planck Collaboration et al., 2013b, preprint (arXiv:1303.5076)
Planck Collaboration et al., 2013c, preprint (arXiv:1303.5084)
Planck Collaboration et al., 2013d, preprint (arXiv:1303.5081)
Press W. H., Schechter P., 1974, ApJ, 187, 425
Prokhorov D. A., Moraghan A., Antonuccio-Delogu V., Silk J., 2012, MNRAS, 425, 1753
Refregier A., Teyssier R., 2002, Phys. Rev. D, 66, 043002
Refregier A., Komatsu E., Spergel D. N., Pen U.-L., 2000, Phys. Rev. D, 61, 123001
Rephaeli Y., 1995, ApJ, 445, 33
Roncarelli M., Moscardini L., Borgani S., Dolag K., 2007, MNRAS, 378, 1259
Roncarelli M., Moscardini L., Branchini E., Dolag K., Grossi M., Iannuzzi F., Matarrese S., 2010, MNRAS, 402, 923

Roychowdhury S., Ruszkowski M., Nath B. B., Begelman M. C., 2004, ApJ, 615, 681

Roychowdhury S., Ruszkowski M., Nath B. B., 2005, ApJ, 634, 90

Salopek D. S., Bond J. R., 1990, Phys. Rev. D, 42, 3936

Scannapieco E., Thacker R. J., Couchman H. M. P., 2008, ApJ, 678, 674

Scaramella R., Cen R., Ostriker J. P., 1993, ApJ, 416, 399

Schaeffer R., Silk J., 1988, ApJ, 333, 509

Scoccimarro R., Hui L., Manera M., Chan K. C., 2012, Phys. Rev. D, 85, 083002

Sefusatti E., Crocce M., Pueblas S., Scoccimarro R., 2006, Phys. Rev. D, 74, 023522

Sefusatti E., Crocce M., Desjacques V., 2010, MNRAS, 406, 1014

Seljak U., 2000, MNRAS, 318, 203

Seljak U., 2002, MNRAS, 337, 769

Sheth R. K., Tormen G., 1999, MNRAS, 308, 119

Springel V., 2005, MNRAS, 364, 1105

Springel V., Hernquist L., 2003, MNRAS, 339, 289

Springel V., White M., Hernquist L., 2001a, ApJ, 549, 681

Springel V., White M., Hernquist L., 2001b, ApJ, 562, 1086

Starobinsky A. A., 1980, Phys. Lett. B, 91, 99

Sunyaev R. A., Zeldovich Y. B., 1969, Nat, 223, 721

Sunyaev R. A., Zeldovich Y. B., 1970, Ap&SS, 7, 3

Sunyaev R. A., Zeldovich Y. B., 1972, Comments Astrophys. Space Phys., 4, 173

Sunyaev R. A., Zeldovich I. B., 1980, ARA&A, 18, 537

Sutherland R. S., Dopita M. A., 1993, ApJS, 88, 253

Takada M., Jain B., 2004, MNRAS, 348, 897

Thomas P., Carlberg R. G., 1989, MNRAS, 240, 1009

Tornatore L., Borgani S., Matteucci F., Recchi S., Tozzi P., 2004, MNRAS, 349, L19

Tornatore L., Ferrara A., Schneider R., 2007, MNRAS, 382, 945

Tornatore L., Borgani S., Viel M., Springel V., 2010, MNRAS, 402, 1911

Verde L., 2010, Adv. Astron., 2010, 768675

Verde L., Heavens A. F., Matarrese S., Moscardini L., 1998, MNRAS, 300, 747

Verde L., Heavens A. F., Matarrese S., 2000, MNRAS, 318, 584

Viel M., Branchini E., Dolag K., Grossi M., Matarrese S., Moscardini L., 2009, MNRAS, 393, 774

Wagner C., Verde L., Boubekeur L., 2010, J. Cosmol. Astropart. Phys., 10, 22

White S. D. M., Rees M. J., 1978, MNRAS, 183, 341

White M., Hernquist L., Springel V., 2002, ApJ, 579, 16

Wilson M. J. et al., 2012, Phys. Rev. D, 86, 122005

Yoshida N., Abel T., Hernquist L., Sugiyama N., 2003, ApJ, 592, 645

Zaldarriaga M., 2000, Phys. Rev. D, 62, 063510

Zhang P., Pen U.-L., 2001, ApJ, 549, 18

Zhang P., Pen U.-L., Wang B., 2002, ApJ, 577, 555

This paper has been typeset from a TEX/LATEX file prepared by the author.